catalysts

MDPI

Article

Catalytic Cracking of Heavy Crude Oil over Iron-Based Catalyst Obtained from Galvanic Industry Wastes

Estefanía Villamarin-Barriga [1], Jéssica Canacuán [1], Pablo Londoño-Larrea [1], Hugo Solís [1], Andrés De La Rosa [1], Juan F. Saldarriaga [2] and Carolina Montero [1,*]

[1] Chemical Engineering Faculty, Universidad Central del Ecuador, Ritter s/n & Bolivia, Quito 17-01-3972, Ecuador; jevillamarin@uce.edu.ec (E.V.-B.); jessicacanacuan@gmail.com (J.C.); palondono@uce.edu.ec (P.L.-L.); hfsolis@uce.edu.ec (H.S.); adelarosa@uce.edu.ec (A.D.L.R.)

[2] Department of Civil and Environmental Engineering, Universidad de los Andes, Carrera 1Este #19A-40, Bogotá 111711, Colombia; jf.saldarriaga@uniandes.edu.co

* Correspondence: cdmontero@uce.edu.ec; Tel.: +593-22544361

Received: 2 June 2020; Accepted: 17 June 2020; Published: 3 July 2020

Abstract: Sewage sludge from the galvanic industry represents a problem to the environment, due to its high metal content that makes it a hazardous waste and must be treated or disposed of properly. This study aimed to evaluate the sludge from three galvanic industries and determine its possible use as catalysts for the synthesis of materials. Catalyst was obtained from a thermal process based on dried between 100–120 °C and calcination of sludges between 400 to 700 °C. The physical–chemical properties of the catalyst were analyzed by several techniques as physisorption of N_2 and chemisorption of CO of the material. Catalytic activity was analyzed by thermogravimetric analysis of a thermo-catalytic decomposition of crude oil. The best conditions for catalyst synthesis were calcination between 400 and 500 °C, the temperature of reduction between 750 and 850 °C for 15 min. The catalytic material had mainly Fe as active phase and the specific surface between 17.68–96.15 $m^2 \cdot g^{-1}$, the catalysts promote around 6% more weight-loss of crude oil in the thermal decomposition compared with assays without the catalyst. The results show that the residual sludge of galvanic industries after thermal treatment can be used as catalytic materials due to the easiness of synthesis procedures required, the low E-factor obtained and the recycling of industrial waste promoted.

Keywords: sludge; catalytic material; galvanic industry; waste valorization

1. Introduction

The generation of waste worldwide for 2016 was estimated at 2.01 billion tons, while the world generation is expected to reach 3.30 billion $t \cdot day^{-1}$ by 2100 [1]. The global trend shows that industrial waste generation is almost 18 times higher than municipal waste. Industrial waste increases significantly as income level increases [1]. Among these is the waste from the galvanic industry, which produces on average in the United States about 150,000 $t \cdot year^{-1}$ [2], similar values are reported by the European Union [3]. Sludge represents approximately 25 m^3 for every million tons of textile wastewater and two-thirds of these sludges have physicochemical properties that can be modified [4,5].

The recovery of galvanic baths is beneficial in the mechanical industry to avoid corrosion problems in materials [6]. Nevertheless, it generates hazardous industrial waste as the residual sludge of the process baths, mainly from rinsing in the stages of stripping and degrease [7].

Since galvanic sludge wastes are hazardous due to their chemical composition, they need final treatment or disposal in a safe landfill. Worldwide the implemented skills are mainly: disposal in

soils, thermal treatments as pyrolysis/incineration [8–11], encapsulation [12], as a component of other solid materials [3,7,13–15]. Similarly, some techniques as inertization of heavy metals present in this type of sludge have been studied [2]. However, these treatments represent additional costs for galvanic companies.

The sludge of the galvanic industry has been mainly treated by thermochemical processes such as pyrolysis and incineration. The byproducts of this process have been used as adsorbents [5,16]. Due to the diverse metallic content of this residual industrial sludge, there is the possibility of recovering these residues for the synthesis of catalysts [15,17–20]. Sludge obtained from waste from textile industries, aluminum, galvanic and tannery can be converted on a catalyst for the oxidation of the propane, getting conversions of more than 95% [21,22].

Catalysts prepared from the sludge of the process of ferrite were tried for CO conversion, the results indicate that the Cu-ferrite catalyst can convert CO to CO_2 at an inlet CO concentration of 4000 ppm and a space velocity of 6000 h^{-1} were held at 140 °C [23]. The selective catalytic NO reduction was studied using metal catalyst doped with carbon from the residual sludge of ferrite, at 300 °C conversion >99.7% of NO was reported [24]. The sludge waste from wastewater treatment in the textile industries has metals like Fe and Cr were used as catalytic materials during their reducing phase for the decomposition of hydrocarbons [25]. Fe–char catalyst from tank cleaning oily sludge for the catalytic cracking of oily sludge at 800 °C, the oil conversion efficiency reached is around 95.8% [26]. Carbon–silica derived from SiC–Si sludge has been proven as support for Fe catalysts; better results are shown when Fe was loaded by chemical vapor infiltration than incipient wetness impregnation [27]. Metallic iron from the dyeing sludge ash was probed as a catalyst for biomass gasification. It showed similar behavior that of the commercially available iron–chrome-based catalyst for the same equivalent total amount of Fe_2O_3 [28].

This work has aimed to evaluate residual sludge from the galvanic industry as catalysts for which this work raises the synthesis of catalytic materials applied in the reactions of cracking of heavy crude oil.

2. Results and Discussion

2.1. Sludge and Catalyst Characterization

The thermal treatment (calcination) provided the catalytic characteristics at the residual sludge as the drying of the internal water, volatile substances. The metallic content in the sludge was oxidized in this process. Elemental analysis was done to evaluate the organic material eliminated by calcination.

The results of the elemental analysis and physical properties of the dried sludges and catalytic material obtained are shown in Table 1. With a prior drying process can be observed that the optimal drying temperature is 120 °C for L1 and L2 and 100 °C for L3, the differences in the drying temperature can be due at the presence of different compounds and additives on the sludges [29–31].

There was observed that thermal treatment promotes changes in the physical–chemical composition of raw sludge. A higher quantity of sulfur was detected on C3, probably due to the use of sulfuric acid and other sulfur compounds in the galvanic process, with the increase of temperature, these compounds could be converted in oxides [32]. On the C1 and C2 catalyst, the sulfur content was constant. From L2 and its derived catalytic material C2, the content of carbon is higher than the others. It could be due to carbonates and surfactants used on the stripping process [33]. Carbon and sulfur values are low compared with the reported by other authors in this type of sludge, finding carbon content between 25% to 40% and for sulfur between 4% and 22% [5,13,16].

Table 1 shows the effects of calcination temperature on the reduction of surface area and pore volume of catalytic materials. The decrease of surface area can be associated with the collapse of the pore structure [21,34]. The catalyst with the highest surface area was C1. For calcination temperature of 400 °C, the three catalysts showed more upper surface area than the other temperatures, but the high organic content can decrease the catalytic activity. Due to the low surface area, the samples calcined

at 700 °C have not been used on the catalytic activity test because the physisorption capability can be disfavored.

Table 1. Elemental analysis and physical properties of dried residual sludges (L1–L3) and catalytic material synthesized (C1–C3).

Sample	T, °C	% N	% C	% H	% S	Surface Area, $m^2 \cdot g^{-1}$	Pore Volume, $cm^3 \cdot g^{-1}$	E-Factor
L1	120	0.10	2.36	2.05	0.94	nm	nm	nm
C1	400	0.02	0.65	0.35	0.39	96.15	0.12	0.1
	500	0.05	0.44	0.19	0.38	71.37	0.10	
	700	0.03	0.16	0.08	0.35	14.98	0.02	
L2	120	0.15	6.48	0.52	0.20	nm	nm	nm
C2	400	0.02	5.48	0.18	0.22	73.46	0.10	0.1
	500	0.03	5.48	0.14	0.23	63.36	0.09	
	700	0.01	4.77	0.08	0.20	27.56	0.03	
L3	100	1.11	5.86	1.35	2.94	nm	nm	nm
C3	400	0.04	1.74	0.08	3.71	29.72	0.03	0.3
	500	0.03	0.40	0.08	4.23	17.68	0.02	
	700	0.02	0.20	0.06	4.42	4.53	0.01	

nm: not measured.

To determinate the sustainability of this process, the Environmental Factor (E) was calculated [35–37]. E-factor correlates the actual amount of waste produced in the process with the desired product (E = mass of waste/mass of product). In this case, the desired product was the catalyst. The ideal E-factor is zero. The values E-factor are in Table 1; there were between 0.1 and 0.3. This process is sustainable because it can valorize industrial waste minimizing the waste produced in the process [35]. The galvanic companies gave the information that raw sludges had metallic content based on iron and zinc. The MSDS and technical data sheets of the streams on the galvanic processes verified it.

Figure 1 shows the FTIR analysis that allows the identification of functional groups for both sludge and catalytic materials. On L1 and C1 OH groups were observed, probably due to Zn(OH) (1407, 1478 and 1630 cm^{-1}) and other bands in 448 cm^{-1} (Fe_2O_3) and 584 cm^{-1} (Fe_3O_4) [38]. For L2 and C2 were identified bands on 2864 and 875 cm^{-1} correlated with FeOO bond, on 464 cm^{-1} for Fe_2O_3 and 799 cm^{-1} for FeO. The presence of ZnO (606, 712 and 571 cm^{-1}) and Zn(OH) (1801 cm^{-1}) also were detected [39]. Additionally, the band on 448 cm^{-1} identified on L3 and C3 can be associated with $FeSO_4$ [40]. In the sludges, it was observed other peaks at 2923 and 3373 cm^{-1}, related to OH bonds due to the presence of the Fe–Zn hydroxyl groups on the surface [41], these bonds decrease its intensity while the calcination temperature increases.

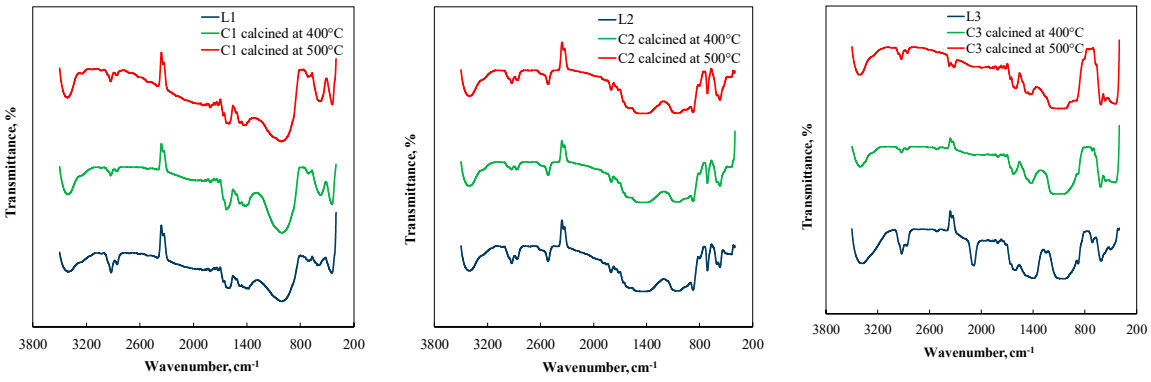

Figure 1. Fourier transform infrared spectroscopy (FTIR) spectra of galvanic sludge and catalytic material.

2.2. Catalyst Reducibility Analysis

The reducibility capability of the synthesized catalysts was studied using the reduction at program temperature (TPR) with hydrogen as a reduction agent, H_2–TPR profiles are shown in Figure 2. C1 and C2 catalysts show three regions for reduction: the first region around 300–550 °C, the second and the prominent area around 550–800 °C, while the third region located between 800–900 °C. In the case of C3 shows only one prominent peak at 650 °C.

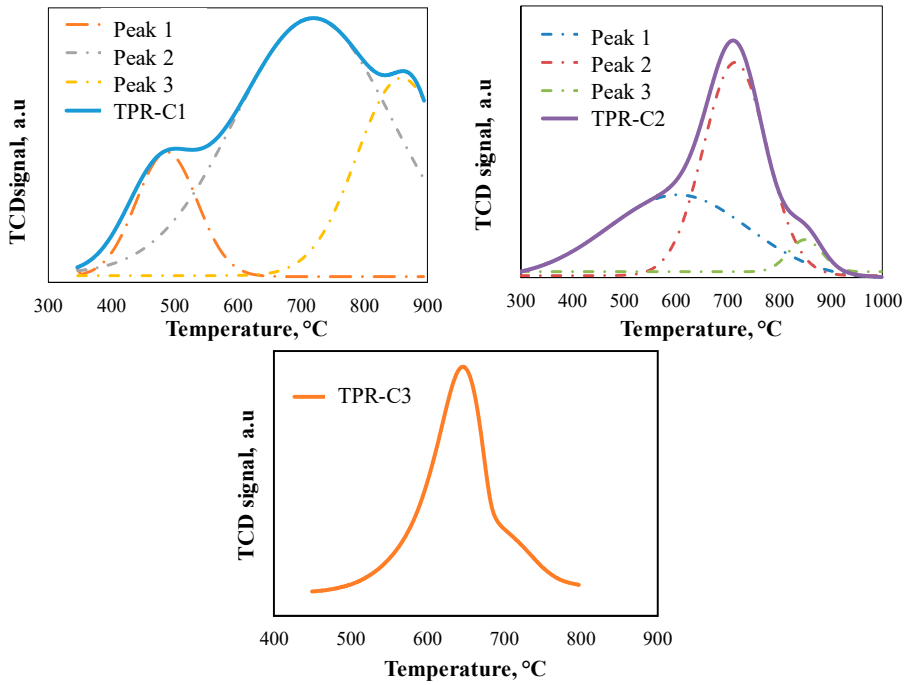

Figure 2. Temperature-programmed reduction (TPR) profile for C1, C2 and C3 calcined at 500 °C.

Similar behavior has been shown for other Fe based catalysts, for Fe/Al_2O_3 catalyst. Other authors have shown the same three areas that were evidenced in this work. The first one between 250–460 °C that can be described as a transformation towards Fe_2O_3, a second region that is between 480–800 °C that the authors associate with Fe_3O_4 formation. Moreover, the last area that is between 830–950 °C, which is related to the Fe formation [42,43].

Likewise, in this work, the second region again is dominant, but concluded that the area could be ascribable at Fe or Zn sulfides. The first region only is present when the Fe sulfides are doped with Zn and the third region increases at the same time, more content of zinc was loaded. Concerning catalyst C3, a particular behavior was found, since the presence of Zn significantly displaced the temperature towards a higher temperature for C1 and C2, this behavior is similar to other studies [44]. Therefore, the reduction peak of ZnO to a metallic state is around 700 °C, but interactions with sulfur compounds can change the reduction temperature at about 650 °C [45]. With this analysis is inferred that the C1–C2 mainly had iron phases while C3 has Fe–Zn.

Figure 3 shows a study of the time influence on the reducibility of the catalyst. The catalysts were analyzed at three different times, 15, 30 and 45 min. The reduction was made at 750 °C for C1, at 850 °C for C2 and 800 °C for C3 to compare the reducibility at different temperatures. In this test, the same behavior of the previous analysis is evidenced, in which the three catalysts present the same peaks (Figure 2). On the three catalysts was observed the complete reduction of the metallic phase at 15 min, longer reduction times did not show significantly higher reducibility. These results are important to be able to extrapolate at some point, the process at an industrial scale.

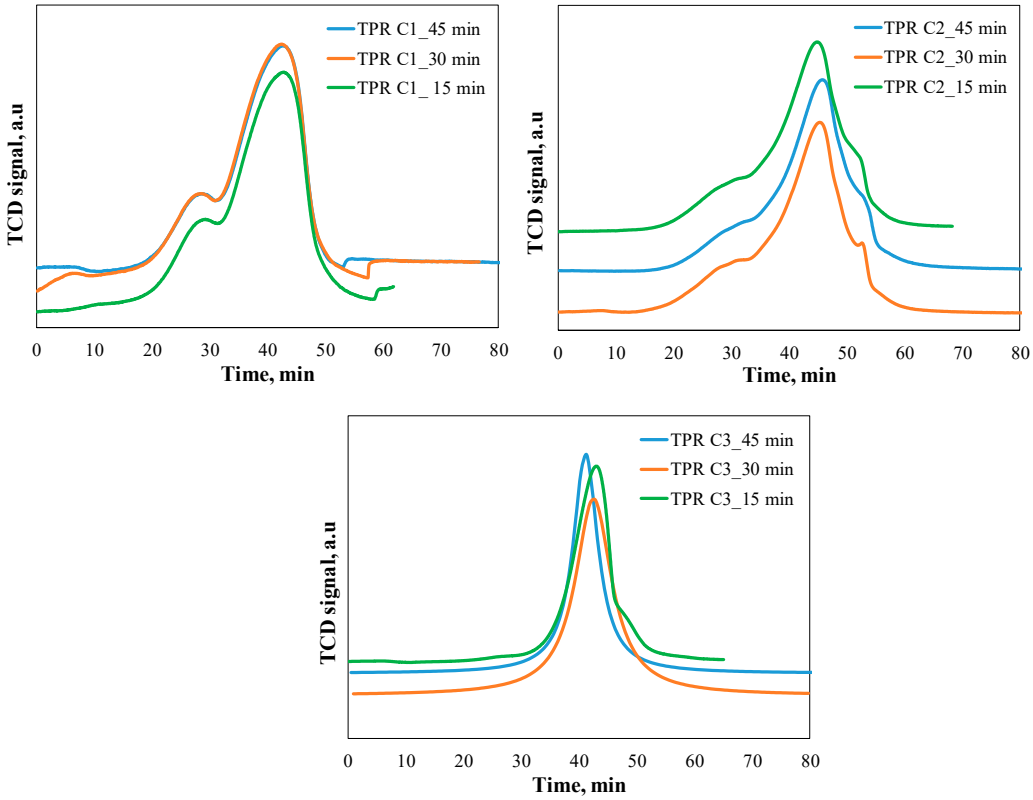

Figure 3. TPR profiles for C1, C2 and C3 at different reduction times on stream.

2.3. Metallic and Textural Properties of the Catalytic Material

The calcined catalyst and the raw sludge were not analyzed through X-ray diffraction (XRD). A similar metallic composition was found in the TPR analysis and while for catalysis application, the synthesized material was reduced. In the case of the reduced catalyst, an XRD analysis was performed. Peak identification was completed with the platform AtomWork: Inorganic Materials Database from NIMS Materials Database (National Institute for Materials Science, Tsukuba, Ibaraki, Japan) [46].

XRD patterns are shown in Figure 4, C1 and C2 had similar patterns, but in the C3, more quantity of peaks had appeared. In the three catalysts were observed mainly peaks corresponding to iron structures and other structures as Zn were defined by FTIR [47–53].

Sulfide structures as FeS (2θ = 26.8, 28.5, 32.85°) were identified in three catalysts, but in C3, ZnS (2θ = 30.5°) were identified too. This compound agreed with the sulfur content quantified in the elemental analysis; for this reason, the peaks in C3 were better defined.

ZnO structures were present in all the catalysts (2θ = 31.7, 34.28°), but C3 had more presence of this structure peaks than the other catalysts (2θ = 47.49, 56.52, 62.8, 67.9 and 72.7°), ZnO_2 (2θ = 41.23°) on C2 and C3, but Zn0 peak (2θ = 36.23°) were seen only in C3. The principal presence in the Zn structures in C3 could be associated with the TPR analysis, in which a single main peak was evident, due to the presence of these structures. In the case of the other two catalysts, the behavior was different because it presented three reduction regions.

Different iron structures were identified in the three catalysts analyzed. Fe_3O_4 (2θ = 35.5°) were found in C1, Fe_2O_3 (2θ = 39.67°) were identified in C2 and FeO (2θ = 50.50, 51.5°), while for C3 the three iron compounds Fe_3O_4 (2θ = 35.5°), Fe_2O_3 (2θ = 39.67°) and FeO (2θ = 50.50, 51.5°) were evidenced. The main peak of FeO (2θ = 44.6, 65.1°) was prominent in C1 and C2, while in the case of C3 was decomposed in two lower peaks. Of the three catalysts, C2 had a lower intensity compared to the other two catalysts.

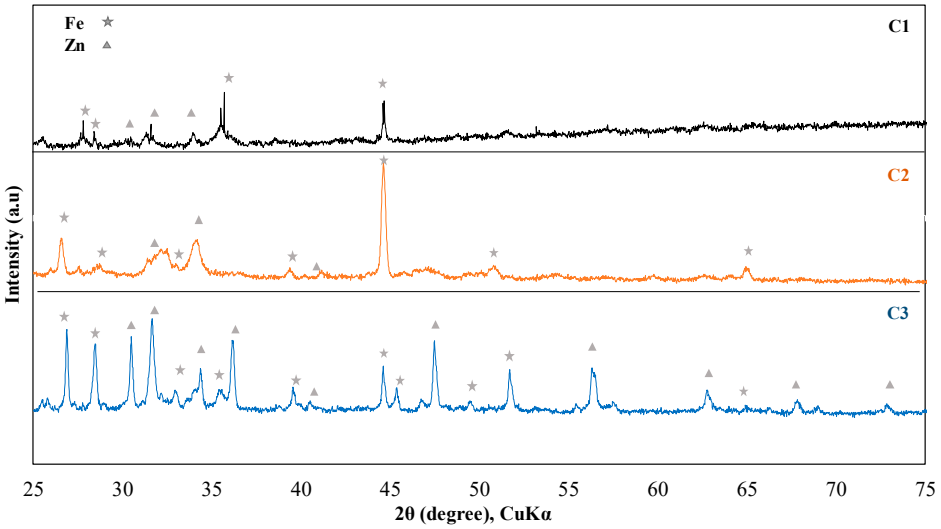

Figure 4. XRD patterns of reduced catalysts C1, C2 and C3.

Scanning electron microscopy-energy dispersive spectrometry (SEM-EDS) confirmed the presence of these metallic phases on the catalytic material. On the surface of C1 were quantified 41.65% Fe and 16.91% Zn, C2 has 19.56% Fe and 7.33% Zn, while C3 has 7.22% Fe and 33.26% Zn. The results were concordant with XRD element identification. The surface morphology of the catalysts by SEM microscopy is shown in Figure 5.

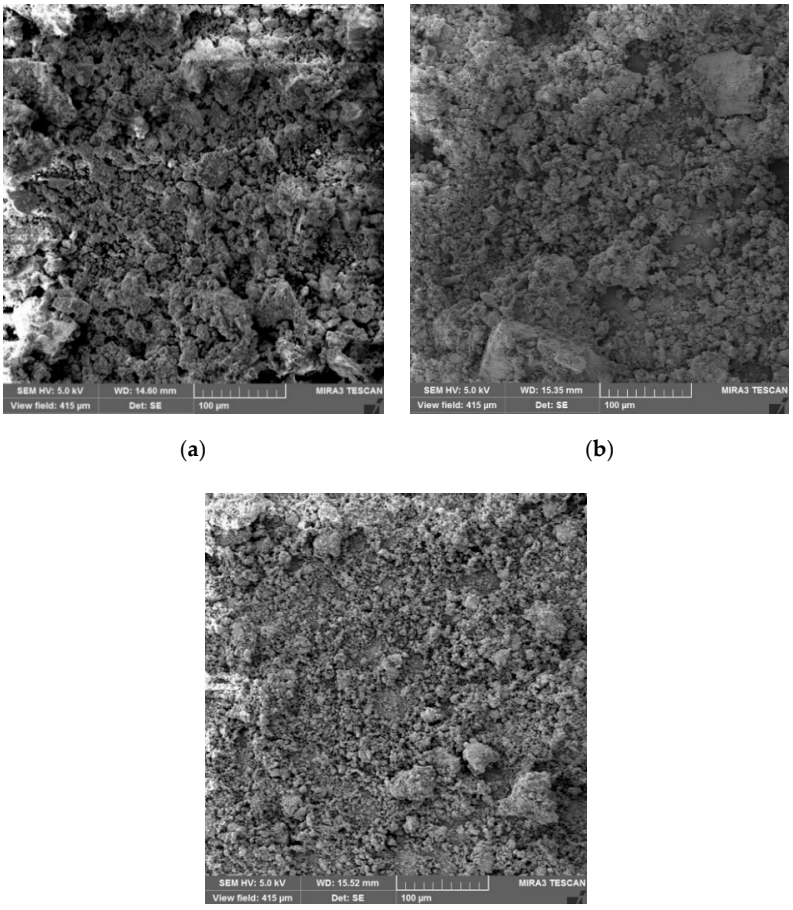

Figure 5. SEM images of C1 (**a**), C2 (**b**) and C3 (**c**) calcined at 550 °C (view at 500×).

No homogeneous particles can be observed in C1–C2, while for C3, it can see some regularity size. Similarly, no crystal-defined structures of catalytic material were found in any of the catalysts evaluated. It may be due to the low homogeneity of the raw sludge. Likewise, differences in morphology between C1 and C3 can be seen, which may be related to the differences in the evaluated surface areas, 96.15 and 17.68 $m^2 \cdot g^{-1}$, respectively (Table 1). To obtain irregular particles with good crystallinity is needed high reaction temperature of 1050 °C [54], but this temperature can cause sinterization for catalyst purposes.

2.4. Catalytic Evaluation of the Synthesized Materials

The chemisorption capacity of the catalytic material was analyzed with CO pulses (Figure 6). This information is important to identify catalytic applications correlated at the CO conversion. For catalysts C1 and C2, it was observed that both could adsorb CO. It is evident that in both the saturation of the surface is in the third pulse, around 10 min. In addition, the adsorption rate is similar for C1 and C2. Therefore, these could be used in CO reactions.

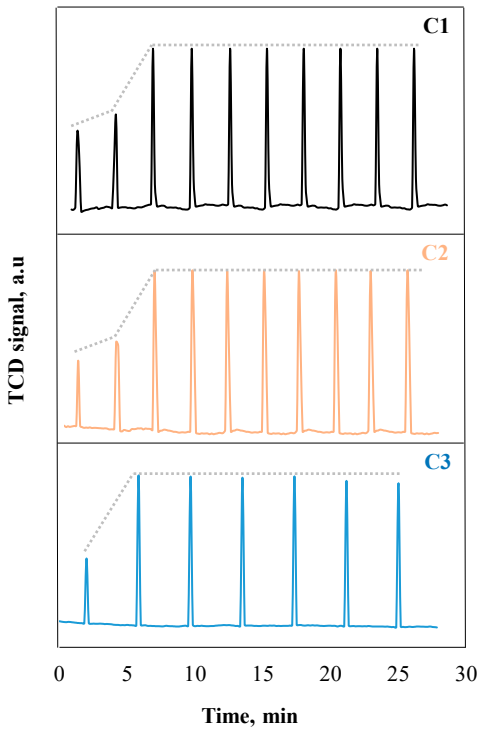

Figure 6. Thermal conductivity detector (TCD) response to CO pulse chemisorption by C1, C2 and C3. C1 and C2 saturation reached after 2 peaks (10 min), C3 saturation reached after 1 peak (3 min).

A different behavior was found for C3. The first time it was not possible to detect any signal. The CO flux was increased, observing a rapid saturation on the second peak around 3 min, a shorter time than in the other two catalysts. This behavior could be attributed to the Zn content compared to the other two that the main compound is iron. In addition, another factor is its low specific surface.

Therefore, this catalyst, C3, does not have characteristics to be used as a catalyst in CO processes.

The catalytic activity of the synthesized materials was analyzed in a reaction to the thermal decomposition of heavy crude oil. The reaction was carried out by thermogravimetric analysis (TGA) in an N_2 atmosphere. This technique has been used previously to characterize the heavy crude oils [55–57].

The loss of mass is considered as indicative of catalytic decomposition, where higher mass-loss on crude oil was regarded as better catalytic activity. These assays were compared with reactions without catalyst and a reaction performed with a commercial catalyst (FCC type, 265 $m^2 \cdot g^{-1}$) at the

same space–time (0.15 g catalyst g^{-1} crude oil). The results are in Table 2; all the catalysts promote the weight-loss while the temperature increases as expected.

Table 2. Effect of the catalyst on the weight loss of crude oil on the thermal decomposition reaction.

Temperature of Reaction, °C	Sample	Weight Loss, %	Kinetic Expression	R^2	Rate of Mass Loss (avg.), mg·min^{-1}
400	Crude oil without catalyst	54.30	$\frac{dm}{dt} = 0.0015\ m_A^{0.5}$	0.90	0.57
	Crude oil + C1	59.28	$\frac{dm}{dt} = 0.0017\ m_A^{0.5}$	0.92	0.61
	Crude oil + commercial cat.	56.00	$\frac{dm}{dt} = 0.0020\ m_A^{0.5}$	0.95	0.65
450	Crude oil without catalyst	73.20	$\frac{dm}{dt} = 0.0016\ m_A^{0.5}$	0.91	0.64
	Crude oil + C2	84.50	$\frac{dm}{dt} = 0.0018\ m_A^{0.5}$	0.90	0.71
	Crude oil + C3	82.10	$\frac{dm}{dt} = 0.0019\ m_A^{0.5}$	0.92	0.69
	Crude oil + commercial cat.	77.95	$\frac{dm}{dt} = 0.0019\ m_A^{0.5}$	0.94	0.81

dm, differential mass; dt, differential time; mA, mass at time (t), mg.

The three catalysts promote around 5% more mass-loss than the experiment without catalyst and some higher mass-loss compared with a commercial catalyst (C2–C3). For C2 and C3, the mass-loss was enhanced at temperatures higher than 400 °C. The catalytic effect was analyzed by mass-loss data, and it was used to define a kinetic model. The kinetic analysis was done applying the integral method of linearization of kinetic expression 2 $m^{0.5}$ vs. time. The kinetic order of 0.5 provided the best fit with the experimental data according to the determination coefficient (R^2).

The average rate of mass loss was calculated for the reactions. The experimental data were replaced in the kinetic expression for each time. The numerical value at $\left(\frac{dm}{dt}\right)$ was obtained for the extension of reaction.

Kinetic expressions showed that the rate of thermal decomposition promoted by catalytic material derived from sludge had similar values than the commercial catalyst, and an evident higher rate than the test without a catalyst, mainly in C2 and C3 to the reaction at 450 °C. For a technical limitation due to the highly exothermic reaction presented by crude oil itself, it was not able to perform thermal decomposition experiments above 450 °C.

These results permit concluded that the catalyst can be used in cracking applications to replace commercial catalysts.

3. Materials and Methods

The samples of sludges were taken from three galvanic companies with similar technologies located in Quito, Ecuador (Table 3). For company 1 the sludge was named L1; for company 2, L2 and company 3, L3. The catalytic materials derived from the sludges were identified as C1, C2 and C3.

Table 3. Nomenclature used for the different sludges evaluated.

Company	Sludge	Catalytic Material
Company 1	L1	C1
Company 2	L2	C2
Company 3	L3	C3

All the analyses of characterization were performed in triplicate to guarantee the best possible results.

3.1. Catalytic Preparation

The residual sludges were dried as is described on ASTM-D2216 in a drying oven (Nabertherm-TR60, Bahnhofstr, Lilienthal, Germany) for 4 h. The dried sludges were sieved between 150–180 μm with a Tyler's-sieve series.

The residual sludges were calcined between 400–700 °C for 4 h in a muffle furnace (Thermo Scientific- Thermolyne, Waltham, MA, USA). This process was done to remove the organic residues and to oxidize the metallic phase on the sludges. After the thermal process, the residual sludges were considered as catalytic material.

The sludges and the catalytic material were analyzed by elemental analysis based on the ASTM-D5373 to identify the organic material in an elemental analyzer (Elementar-Vario Macro Cube, Langenselbold, Germany). Around 10 mg of the sample was exposed to oxidative decomposition at 1150 °C and subsequent reduction at 850 °C, to quantify carbon, hydrogen, nitrogen and sulfur (CHNS) composition. Before the experiment, the samples were prepared by digestion microwave system (Milestone-ETHOS UP, Sorisole, BG, Italy).

Fourier-transformed infrared spectroscopy (FTIR) (PerkinElmer-Spectrum Two spectrometer, Waltham, MA, USA) was used to identify the bonds related to organic and inorganic compounds on the sludges. The dried samples were pulverized in an agate mortar and then mixed with KBr (PerkinElmer, Waltham, MA, USA), in a weight ratio 1:100. Later, a pellet was formed in a press and then read on FTIR.

3.2. Catalyst Characterization

The surface area and pore volume of the catalytic material were determined by N_2 adsorption–desorption in a surface area analyzer (Horiba-SA 9600, minami-ku, Kyoto, Japan). The equipment uses the flowing gas method to acquire gas adsorption and desorption curves, and the surface area was by the single-point BET method. A sample of 0.15 g was loaded in a *U*-tube and degasified for 2 h at 300 °C to clean the surface. Later, the N_2 adsorption–desorption was done using liquid N_2 (Enox S.A, Quito, Pichincha, Ecuador).

Temperature-programmed reduction (TPR) was done to study the reducibility of the catalysts in an automated chemisorption analyzer (Micromeritics-AutoChem II, 2920, Norcross, GA, USA). The catalyst samples (200 mg) were reduced at the heating rate of 10 °C·min^{-1} up 1000 °C under a flow (50 mL·min^{-1}) of 10% H_2/Ar (99.999%, INDURA, Quito, Pichincha, Ecuador). The consumption of hydrogen was monitored with a thermal conductivity detector (TCD). Experiments were performed at 15, 30 and 45 min to define the effect to the time on the total reduction.

X-ray diffraction was done (Malvern Panalytical-Empyrean, Malvern Worcestershire, UK) with CuKα radiation source and Scanning electron microscopy SEM/EDS in a (TESCAN-MIRA3 FEG SEM, Brno, Kohoutovice, Czech Republic) were used to study the metallic content on the reduced catalyst. These assays were done in an external laboratory CENCINAT ESPE Laboratory (Sangolquí, Pichincha, Ecuador).

3.3. Catalytic Material Evaluation

The CO chemisorption was studied with CO pulses technique (Micromeritics-AutoChem II, 2920, Norcross, GA, USA). Before the experiments, the catalysts were reduced, as described previously. Chemisorption experiments were done with 200 mg of the samples at 50 °C [58] exposed at the catalyst at 10% CO/He (99,999%, INDURA, Quito, Pichincha, Ecuador). The total adsorption amount of CO was detected by TCD. The gas uptake was measured from a sequence of small pulses until saturation was obtained.

The catalytic activity of the synthesized materials was evaluated with a thermal decomposition reaction with a crude oil sample (18.9 °API, PETROECUADOR, Esmeraldas, Esmeraldas, Ecuador). A thermogravimetric analysis in a thermo-balance (Mettler Toledo-TGA1 SF/1100, Columbus, OH, USA),

was realized in a reaction atmosphere of N_2 (30 mL·min^{-1}, 99,999%, INDURA, Quito, Pichincha, Ecuador) to determine the loss of mass promoted for the catalytic activity. In this assay, a space–time of 0.15 g catalyst g^{-1} crude oil was used. The studies were performed at 400 °C for C1 and 450 °C for C2–C3 with a rate of heating to 10 °C·min^{-1}. The reaction had 1 h to time on stream and the mass loss was recorded every 35 s.

Before the study, the catalytic material was reduced in a 10% H2/Ar. Assays without catalyst and FCC commercial catalyst (GRACE-ResidCrackeR, Columbia, MD, USA) were done to compare the catalytic effect on the crude oil. The reaction rate of thermo-catalytic decomposition was determined through the integral method of data analysis considering the loss of mass vs. time of reaction.

4. Conclusions

Due to the metal content—mainly iron in their composition—sludge from wastewater treatment from galvanic industries can be used as catalytic material in the thermal decomposition of hydrocarbons—after a thermal treatment.

The best catalytic activity was evidenced at the sludges calcinated at 400 °C for C1 and 500 °C for C2–C3. The catalysts had specific surface areas of 96.15, 63.36 and 17.68 m^2·g^{-1}, respectively. For the reduction of the catalyst, the best condition of time was 15 min and 750, 850 and 800 °C for C1, C2 and C3, respectively. The prepared catalyst evidenced at CO chemisorption capacity, those with the best performance were catalysts C1 and C2.

The catalytic material enhanced the rate of reaction on the thermal decomposition of crude oil promotes more weight-loss in a thermo-gravimetric analysis compared to the reactions without the catalyst.

The synthesis presented here is a good and sustainable alternative to commercial (heavy oil cracking) catalysts due to the easiness of synthesis procedures required, the low E-factor obtained and the recycling of industrial waste promoted.

Author Contributions: Conceptualization, C.M., H.S. and A.D.L.R.; methodology, C.M., H.S. and A.D.L.R.; validation, C.M., H.S. and A.D.L.R.; formal analysis, E.V.-B., J.C., P.L.-L. and C.M.; investigation, E.V.-B., J.C., P.L.-L. and C.M.; resources, C.M. and A.D.L.R.; data curation E.V.-B., J.C. and P.L.L.; writing—original draft preparation, C.M., E.V.-B., A.D.L.R., P.L.-L. and J.F.S.; writing—review and editing, C.M., H.S. and J.F.S.; visualization, C.M., H.S. and A.D.L.R.; supervision, C.M.; project administration, C.M.; funding acquisition, C.M. and A.D.L.R. All authors have read and agreed to the published version of the manuscript.

Funding: This work was carried with the financial support of the Central University of Ecuador (UCE)—Advanced Projects Program 2017, Project N° 23.

Acknowledgments: The authors are grateful to the Chemical Engineering Faculty (UCE) for the lab facilities and J. Alvear from Laboratory of Catalyst (FIQ-UCE) for her technical assistance. Juan F. Saldarriaga thanks to Dept. Civil and Environmental Engineering of the Universidad de los Andes.

Conflicts of Interest: The authors declare no conflict of interest.

References

1. Kaza, S.; Yao, L.C.; Bhada-Tata, P.; Van Woerden, F. *What a Waste 2.0: A Global Snapshot of Solid Waste Management to 2050*; Urban Development; World Bank: Washington, DC, USA, 2018.
2. Mymrin, V.; Borgo, S.C.; Alekseev, K.; Avanci, M.A.; Rolim, P.H.B.; Argenda, M.A.; Klitzke, W.; Gonçalves, A.J.; Catai, R.E. Galvanic Cr-Zn and spent foundry sand waste application as valuable components of sustainable ceramics to prevent environment pollution. *Int. J. Adv. Manuf. Technol.* **2020**, *107*, 1239–1250. [CrossRef]
3. Pérez-Villarejo, L.; Martínez-Martínez, S.; Carrasco-Hurtado, B.; Eliche-Quesada, D.; Ureña-Nieto, C.; Sánchez-Soto, P.J. Valorization and inertization of galvanic sludge waste in clay bricks. *Appl. Clay Sci.* **2015**, *105–106*, 89–99. [CrossRef]
4. Huang, M.; Chen, L.; Chen, D.; Zhou, S. Characteristics and aluminum reuse of textile sludge incineration residues after acidification. *J. Environ. Sci.* **2011**, *23*, 1999–2004. [CrossRef]
5. Sohaimi, K.S.A.; Ngadi, N.; Mat, H.; Inuwa, I.M.; Wong, S. Synthesis, characterization and application of textile sludge biochars for oil removal. *J. Environ. Chem. Eng.* **2017**, *5*, 1415–1422. [CrossRef]

6. Cagno, E.; Trucco, P. Cleaner technology transfer in the Italian galvanic industry: Economic and know-how issues. *J. Clean. Prod.* **2008**, *16*, S32–S36. [CrossRef]
7. Stepanov, S.; Morozov, N.; Morozova, N.; Ayupov, D.; Makarov, D.; Baishev, D. Efficiency of Use of Galvanic Sludge in Cement Systems. *Procedia Eng.* **2016**, *165*, 1112–1117. [CrossRef]
8. Svoboda, K.; Baxter, D.; Martinec, J. Nitrous oxide emissions from waste incineration. *Chem. Pap.* **2006**, *60*, 78–90. [CrossRef]
9. Werle, S. A reburning process using sewage sludge-derived syngas. *Chem. Pap.* **2012**, *66*, 99–107. [CrossRef]
10. Rossini, G.; Bernardes, A.M. Galvanic sludge metals recovery by pyrometallurgical and hydrometallurgical treatment. *J. Hazard. Mater.* **2006**, *131*, 210–216. [CrossRef]
11. Cichowicz, R.; Stelęgowski, A. Effect of thermal sludge processing on selected components of air quality in the vicinity of a wastewater treatment plant. *Chem. Pap.* **2019**, *73*, 843–849. [CrossRef]
12. Castañeda Bocanegra, J.J.; Espejo Mora, E.; Cubillos González, G.I. Encapsulation in ceramic material of the metals Cr, Ni, and Cu contained in galvanic sludge via the solidification/stabilization method. *J. Environ. Chem. Eng.* **2017**, *5*, 3834–3843. [CrossRef]
13. Felisberto, R.; Santos, M.C.; Arcaro, S.; Basegio, T.M.; Bergmann, C.P. Assessment of environmental compatibility of glass–ceramic materials obtained from galvanic sludge and soda–lime glass residue. *Process Saf. Environ. Prot.* **2018**, *120*, 72–78. [CrossRef]
14. Luz, C.A.; Rocha, J.C.; Cheriaf, M.; Pera, J. Valorization of galvanic sludge in sulfoaluminate cement. *Constr. Build. Mater.* **2009**, *23*, 595–601. [CrossRef]
15. Bednarik, V.; Vondruska, M.; Koutny, M. Stabilization/solidification of galvanic sludges by asphalt emulsions. *J. Hazard. Mater.* **2005**, *122*, 139–145. [CrossRef] [PubMed]
16. Wong, S.; Yac'cob, N.A.N.; Ngadi, N.; Hassan, O.; Inuwa, I.M. From pollutant to solution of wastewater pollution: Synthesis of activated carbon from textile sludge for dye adsorption. *Chin. J. Chem. Eng.* **2018**, *26*, 870–878. [CrossRef]
17. Amaral, F.A.D.; dos Santos, V.S.; Bernardes, A.M. Metals recovery from galvanic sludge by sulfate roasting and thiosulfate leaching. *Miner. Eng.* **2014**, *60*, 1–7. [CrossRef]
18. Huyen, P.T.; Dang, T.D.; Tung, M.T.; Huyen, N.T.T.; Green, T.A.; Roy, S. Electrochemical copper recovery from galvanic sludge. *Hydrometallurgy* **2016**, *164*, 295–303. [CrossRef]
19. Jandová, J.; Štefanová, T.; Niemczyková, R. Recovery of Cu-concentrates from waste galvanic copper sludges. *Hydrometallurgy* **2000**, *57*, 77–84. [CrossRef]
20. Silva, J.E.; Paiva, A.P.; Soares, D.; Labrincha, A.; Castro, F. Solvent extraction applied to the recovery of heavy metals from galvanic sludge. *J. Hazard. Mater.* **2005**, *120*, 113–118. [CrossRef]
21. Klose, F.; Scholz, P.; Kreisel, G.; Ondruschka, B.; Kneise, R.; Knopf, U. Catalysts from waste materials. *Appl. Catal. B Environ.* **2000**, *28*, 209–221. [CrossRef]
22. Sushil, S.; Scholz, P.; Pollok, K.; Ondruschka, B.; Batra, V.S. Application of industrial waste based catalysts for total oxidation of propane. *Chem. Eng. J.* **2011**, *166*, 568–578. [CrossRef]
23. Lou, J.-C.; Chang, C.-K. Catalytic Oxidation of CO Over a Catalyst Produced in the Ferrite Process. *Environ. Eng. Sci.* **2006**, *23*, 1024–1032. [CrossRef]
24. Zhang, J.; Zhang, J.; Xu, Y.; Su, H.; Li, X.; Zhou, J.Z.; Qian, G.; Li, L.; Xu, Z.P. Efficient Selective Catalytic Reduction of NO by Novel Carbon-doped Metal Catalysts Made from Electroplating Sludge. *Environ. Sci. Technol.* **2014**, *48*, 11497–11503. [CrossRef] [PubMed]
25. Montero, C.; Castañeda, K.M.; Suntasig, Y.M.O.; Oña, D.R.F.; De La Rosa, A. Catalyst Based on Sludge Derived from Wastewater Treatment of Textile Industry. *Chem. Eng. Trans.* **2018**, *70*, 931–936. [CrossRef]
26. Lin, B.; Huang, Q.; Yang, Y.; Chi, Y. Preparation of Fe-char catalyst from tank cleaning oily sludge for the catalytic cracking of oily sludge. *J. Anal. Appl. Pyrolysis* **2019**, *139*, 308–318. [CrossRef]
27. Lee, M.S.; Park, K.Y.; Park, H.K.; Kang, T.W.; Jang, H.D.; Han, S.S.; Jeon, J.-K. Prospective application of carbon-silica derived from SiC-Si sludge as a support for Fe catalysts. *Korean J. Chem. Eng.* **2017**, *34*, 100–104. [CrossRef]
28. Nam, S.-B.; Park, Y.-S.; Yun, Y.-S.; Gu, J.-H.; Sung, H.-J.; Horio, M. Catalytic application of metallic iron from the dyeing sludge ash for benzene steam reforming reaction in tar emitted from biomass gasification. *Korean J. Chem. Eng.* **2016**, *33*, 465–472. [CrossRef]
29. Zhu, F.; Jiang, H.; Zhang, Z.; Zhao, L.; Wang, J.; Hu, J.; Zhang, H. Research on Drying Effect of Different Additives on Sewage Sludge. *Procedia Environ. Sci.* **2012**, *16*, 357–362. [CrossRef]

30. Ronda, A.; Gómez-Barea, A.; Haro, P.; de Almeida, V.F.; Salinero, J. Elements partitioning during thermal conversion of sewage sludge. *Fuel Process. Technol.* **2019**, *186*, 156–166. [CrossRef]
31. Guangyin, Z.; Youcai, Z. Chapter Three—Sewage Sludge Solidification/Stabilization and Drying/Incineration Process. In *Pollution Control and Resource Recovery for Sewage Sludge*; Guangyin, Z., Youcai, Z., Eds.; Butterworth-Heinemann: Oxford, UK, 2017; pp. 101–160, ISBN 978-0-12-811639-5.
32. Kuzin, E.N.; Chernyshev, P.I.; Vizen, N.S.; Krutchinina, N.E. The Purification of the Galvanic Industry Wastewater of Chromium(VI) Compounds Using Titanium(III) Chloride. *Russ. J. Gen. Chem.* **2018**, *88*, 2954–2957. [CrossRef]
33. Kliopova, I.; Staniškis, J. Optimization of Galvanic Wastewater Treatment Processes. In *Modern Tools and Methods of Water Treatment for Improving Living Standards*; Omelchenko, A., Pivovarov, A.A., Swindall, W.J., Eds.; Springer: Dordrecht, the Netherlands, 2005; pp. 197–208.
34. Torres-Luna, J.A.; Carriazo, J.G.; Sanabria-González, N.R. Calcination Temperature Effect on structural and textural properties of Fe(iii)-TiO_2. *Rev. Fac. Cienc. Básicas* **2014**, *10*, 186–195. [CrossRef]
35. Sheldon, R.A. Fundamentals of green chemistry: Efficiency in reaction design. *Chem. Soc. Rev.* **2012**, *41*, 1437–1451. [CrossRef] [PubMed]
36. Dicks, A.P.; Hent, A. The E Factor and Process Mass Intensity. In *Green Chemistry Metrics: A Guide to Determining and Evaluating Process Greenness*; SpringerBriefs in Molecular Science; Dicks, A.P., Hent, A., Eds.; Springer International Publishing: Cham, Switzerland, 2015; pp. 45–67, ISBN 978-3-319-10500-0.
37. Tieves, F.; Tonin, F.; Fernández-Fueyo, E.; Robbins, J.M.; Bommarius, B.; Bommarius, A.S.; Alcalde, M.; Hollmann, F. Energising the E-factor: The E+-factor. *Tetrahedron* **2019**, *75*, 1311–1314. [CrossRef]
38. Sahoo, S.K.; Agarwal, K.; Singh, A.K.; Polke, B.G.; Raha, K.C. Characterization of γ- and α-Fe_2O_3 nano powders synthesized by emulsion precipitation-calcination route and rheological behaviour of α-Fe_2O_3. *Int. J. Eng. Sci. Technol.* **2010**, *2*. [CrossRef]
39. Ortego, J.D.; Barroeta, Y.; Cartledge, F.K.; Akhter, H. Leaching effects on silicate polymerization. An FTIR and silicon-29 NMR study of lead and zinc in portland cement. *Environ. Sci. Technol.* **1991**, *25*, 1171–1174. [CrossRef]
40. Paterson, E. The Iron Oxides. Structure, Properties, Reactions, Occurrences and Uses. *Clay Min.* **2006**, *34*, 209–210. [CrossRef]
41. Iqbal, A.; Jacob, J.; Mahmood, A.; Mehboob, K.; Mahmood, K.; Ali, A.; Bukhari, T.H.; Adrees, M.; Ibrahim, M.; Ahmad, M. Synthesis and characterization of Zn–Mn–Fe nano oxide composites for the degradation of reactive yellow 15 dye. *Phys. B Condens. Matter* **2020**, *588*, 412210. [CrossRef]
42. Fakeeha, A.; Khan, W.; Ibrahim, A.; Al-Otaibi, R.; Alfatesh, A.; Soliman, M.; Abasaeed, A. Alumina supported iron catalyst for hydrogen production: Calcination study. *Int. J. Adv. Chem. Eng. Biol. Sci.* **2015**, *2*, 139–141. [CrossRef]
43. Li, H.; Liu, J.; Li, J.; Hu, Y.; Wang, W.; Yuan, D.; Wang, Y.; Yang, T.; Li, L.; Sun, H.; et al. Promotion of the Inactive Iron Sulfide to an Efficient Hydrodesulfurization Catalyst. *ACS Catal.* **2017**, *7*, 4805–4816. [CrossRef]
44. Liang, K.; Zhang, C.; Xiang, H.; Yang, Y.; Li, Y. Effects of modified SiO_2 on H_2 and CO adsorption and hydrogenation of iron-based catalysts. *J. Fuel Chem. Technol.* **2019**, *47*, 769–779. [CrossRef]
45. Song, H.; Cui, H.; Li, F. The effect of Zn–Fe modified S_2O_8 2−/ZrO_2–Al_2O_3 catalyst for n-pentane hydroisomerization. *Res. Chem. Intermed.* **2016**, *42*, 3029–3038. [CrossRef]
46. National Institute for Materials Science NIMS Materials Database (MatNavi). Available online: https://mits.nims.go.jp/index_en.html (accessed on 12 May 2020).
47. Glavee, G.N.; Klabunde, K.J.; Sorensen, C.M.; Hadjipanayis, G.C. Chemistry of Borohydride Reduction of Iron(II) and Iron(III) Ions in Aqueous and Nonaqueous Media. Formation of Nanoscale Fe, FeB, and Fe_2B Powders. *Inorg. Chem.* **1995**, *34*, 28–35. [CrossRef]
48. Legodi, M.A.; de Waal, D. The preparation of magnetite, goethite, hematite and maghemite of pigment quality from mill scale iron waste. *Dyes Pigments* **2007**, *74*, 161–168. [CrossRef]
49. Picasso, G.; Sun Kou, R.; Gómez, G.; Hermoza, E.; López, A.; Pina, M.P.; Herguido, J. Nanosized catalyst based on Fe Oxide for combustion of n-hexane. *Rev. Soc. Quím. Perú* **2009**, *75*, 163–176.
50. Caballero, D.; Mass, J.; Landinez, D. Optical and Structural Characterization of Zn_2 TiO_4 capped with Mg. *Tumbaga* **2011**, *6*, 165–172.
51. Kumar, H.; Rani, R. Structural and Optical Characterization of ZnO Nanoparticles Synthesized by Microemulsion Route. *Int. Lett. Chem. Phys. Astron.* **2013**, *14*, 26–36. [CrossRef]

52. Dou, J.; Li, X.; Tahmasebi, A.; Xu, J.; Yu, J. Desulfurization of coke oven gas using char-supported Fe-Zn-Mo catalysts: Mechanisms and thermodynamics. *Korean J. Chem. Eng.* **2015**, *32*, 2227–2235. [CrossRef]
53. Yan, Z.; Kang, Y.; Li, D.; Liu, Y.C. Catalytic oxidation of sulfur dioxide over α-Fe_2O_3/SiO_2 catalyst promoted with Co and Ce oxides. *Korean J. Chem. Eng.* **2020**, *37*, 623–632. [CrossRef]
54. Yin, X.; Yue, M.; Lu, Q.; Liu, M.; Wang, F.; Qiu, Y.; Liu, W.; Zuo, T.; Zha, S.; Li, X.; et al. An Efficient Process for Recycling Nd–Fe–B Sludge as High-Performance Sintered Magnets. *Engineering* **2020**, *6*, 165–172. [CrossRef]
55. Kök, M.V.; Varfolomeev, M.A.; Nurgaliev, D.K. Crude oil characterization using TGA-DTA, TGA-FTIR and TGA-MS techniques. *J. Pet. Sci. Eng.* **2017**, *154*, 537–542. [CrossRef]
56. Simo, S.M.; Naman, S.A.; Ahmed, K.R.; Faritovich, A.A. Evaluation of Two Kurdistan-Iraq Crude Oil (T-21A, PF2) by Derivatographic Method. *Int. Res. J. Pure Appl. Chem.* **2020**, 38–46. [CrossRef]
57. Park, Y.C.; Paek, J.-Y.; Bae, D.-H.; Shun, D. Study of pyrolysis kinetics of Alberta oil sand by thermogravimetric analysis. *Korean J. Chem. Eng.* **2009**, *26*, 1608–1612. [CrossRef]
58. Liu, S.; Ren, J.; Zhu, S.; Zhang, H.; Lv, E.; Xu, J.; Li, Y.-W. Synthesis and characterization of the Fe-substituted ZSM-22 zeolite catalyst with high n-dodecane isomerization performance. *J. Catal.* **2015**, *330*, 485–496. [CrossRef]